Classification of Unresolved Target Based on Specular Reflection.

by

Ahmed Alghamdi

A Dissertation Submitted to the Faculty of the

DEPARTMENT OF OPTICAL SCIENCES

In Partial Fulfillment of the Requirements

For the Degree of

MASTER OF SCIENCE

In the Graduate College

THE UNIVERSITY OF ARIZONA
GRADUATE COLLEGE

As members of the Master's Committee, we certify that we have read the thesis prepared by *Ahmed Saeed Alghamdi* titled *Classification of Unresolved Target Based on Specular Reflection.* and recommend that it be accepted as fulfilling the dissertation requirement for the Master's Degree.

Mohamed ElKabbash — Date: 05/03/2024
Mohamed ElKabbash

Date: 5/3/24
David Brady

Date: 5/3/2024
Brandon Chalifoux

Final approval and acceptance of this thesis is contingent upon the candidate's submission of the final copies of the thesis to the Graduate College.

I hereby certify that I have read this thesis prepared under my direction and recommend that it be accepted as fulfilling the Master's requirement.

Mohamed Elkabbash — Date: 05/03/2024
Mohamed ElKabbash
Master's Thesis Committee Chair
Department of Optical Sciences

ACKNOWLEDGMENTS

Dr. Mohammed, Dr. Brady, and Dr. Chalifoux for all their support and guidance, as well as standing by my side during my hard times. My research team, Gordon and Greg, for their outstanding work in this research. My company STIRA, for giving me this opportunity.

LAND ACKNOWLEDGMENT

We respectfully acknowledge the University of Arizona is on the land and territories of Indigenous peoples. Today, Arizona is home to 22 federally recognized tribes, with Tucson being home to the O'odham and the Yaqui. Committed to diversity and inclusion, the University strives to build sustainable relationships with sovereign Native Nations and Indigenous communities through education offerings, partnerships, and community service.

DEDICATION

My beloved family, whose unwavering support and love have been my cornerstone, and my dear friends at Wyant College of Optics, whose encouragement and companionship have lightened my journey. Above all, to my wife, Your patience, understanding, and boundless support have made all the difference

Thank you all for being part of this journey…

TABLE OF CONTENTS

LIST OF FIGURES

LIST OF TABLES

ABSTRACT

This thesis explores using specular reflections to enhance remote sensing capabilities for identifying unresolved targets. Traditional remote sensing methods often struggle with the resolution limitations imposed by distance and target size, making distinguishing and classifying distant objects difficult. This research proposes a novel approach to overcome these constraints by harnessing the unique properties of specular reflections. Through a series of methodically designed experiments conducted in laboratory settings and real-world scenarios, this study demonstrates the potential of specular reflections to act as optical 'fingerprints.' These experiments validate theoretical models and show the practical applicability of specular reflections for long-range identification and classification tasks. Key experiments included detailed analyses over 27 kilometers, revealing how specular reflections can be captured and analyzed to provide critical data beyond traditional imaging capabilities. The findings of this research have significant implications for military surveillance, environmental monitoring, and space debris tracking, offering a new tool for enhanced observation and identification of distant objects. This thesis proves that specular reflections can extend the visual reach of remote sensing technologies, paving the way for more precise and reliable long-distance optical sensing.

1. Classification of Unresolved Target Based on Specular Reflection

1.1 Introduction

Pursuing advanced optical sensing technologies has become a cornerstone of modern scientific research and technological innovation, with applications spanning from environmental monitoring to national security and beyond. In this dynamic and ever-evolving field, accurately classifying and characterizing targets from significant distances is not just an academic interest but a necessity that snaps multiple disciplines. This thesis introduces pioneering research conducted at the Wyant College of Optical Sciences-University of Arizona, which seeks to address one of the most challenging aspects of remote sensing: the classification of unresolved targets-objects that are not distinctly resolvable by conventional imaging systems due to their distance or small size.

Unresolved targets present a unique challenge in optical sensing, as traditional methods that rely on high-resolution imagery to identify and classify objects become ineffective. The limitations posed by distance and physics of light propagation require innovative approaches to extract usable data from the scant information that reaches sensors. In response to this challenge, our research focuses on exploiting the properties of light itself, particularly examining how light, both specular and diffuse, interacts with different surfaces from a distance.

Specular reflections occur when light bounces off surfaces in such a way that the angle at which the light rays arrive equals the angle at which they depart (Figure 1). While simple in concept, this phenomenon encodes information about the reflecting object's surface geometry and material properties. By analyzing these reflections, particularly in the context of unresolved targets, our research develops methods to extrapolate detailed characteristics about distant objects that are otherwise obscured or invisible in standard imaging techniques.

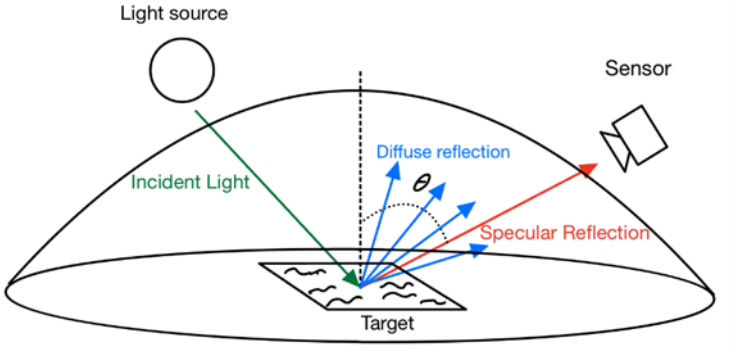

Figure 1: illustration of Specular Reflection. The dome represents the radiance field L.

This study was conducted by a dedicated team of researchers, including Ahmed Alghamdi, Gergory Nero, Gordon Hageman, and Dr. David Brady. It employs a novel approach to decoding the subtle cause within the radiance fields of specular reflections. By sampling and analyzing these radiance fields, we can distinguish between different types of unresolved targets, effectively using light as a diagnostic tool. This method can enhance existing remote sensing capabilities and revolutionize how we observe and interact with distant objects across various sectors.

1.2 Methodological Overview

The unique specular reflection of an object is not only a wealth of information about its shape and surface characteristics but also a potent tool for identification, extending its utility to the domain of remote sensing technology. As the resolution of images captured by remote sensors is often limited by distance, traditional imaging methods may not suffice to resolve small objects like drones. However, by analyzing the pattern of specular reflection, one can conclude identifying characteristics of drones even when they are beyond the resolution limit of the imaging system. The concept hinges on the fact that every object, depending on its geometrical 3d shape, construction materials, and surface finish, will reflect sunlight in a signature pattern. This pattern, though perhaps not resolvable to a clear image, can still be detected and analyzed. Such an approach draws on advanced optics and signal processing topics, where even a single pixel of light-intensity data can be rich in information, provided that the specular reflection is captured and interpreted correctly.

In a scenario where a drone is flying at a distance where it appears as a mere speck to the naked eye or a standard camera, the characteristics of the light it reflects could still identify the drone's presence and type. The reflective signature could reveal not just the drone's presence but potentially its class, size, and even its type. This involves sophisticated computational methods that analyze the changing light intensity over time, extracting patterns that correspond to known drone signatures.

This principle is similar to the methods employed in astronomy to identify celestial bodies. When direct imaging is impossible due to great distances, scientists rely on light curves—graphs of light intensity from a star or planet over time—to identify and characterize them. Analogously, by examining the 'light curve' of a drone's specular reflection, it may be possible to classify the drone accurately.

Security and airspace management applications are evident, where the ability to detect, track, and classify drones at long distances is crucial. This passive remote sensing technique could be employed around sensitive areas such as airports, where drones pose a risk to aircraft. The technique would complement other methods like radar and acoustic detection, offering non-intrusive and potentially more ways of monitoring.

1.3 Detailed Analysis of Specular Reflection

The unique specular reflection of any object could thus serve as a 'fingerprint' from afar, providing a powerful means of identification when direct imaging fails. As technology progresses and computational models become more sophisticated, the potential for using light itself as a means of recognizing and classifying objects, even those as elusive as drones at a distance, becomes increasingly feasible and practical. Faces uniquely scatter light. The simplified approach for the math relies on the following derivation from the Phong model (Equation 2) and then applies it to the radiance (Equation 4).

$$L = \frac{d^2\Phi}{dAd\Omega} \quad (1)$$

$d^2\Phi$ is the differential amount of energy (radiant flux), dA is the differential area perpendicular to the direction of propagation, $d\Omega$ is the differential solid angle.
For specular reflection, which is directional and depends on the surface geometry and the viewing angle, the surface behavior can be modeled as follows:

$$I_p = I_i k_s (\hat{r} \,.\, \hat{v})^n \quad (2)$$

I_p is the intensity of the reflected light, and I_i is the intensity of incident light k_s is the specular reflection coefficient (a material property). $\hat{r}$ is the unit vector in the direction of the perfect reflection. $\hat{v}$ is the unit vector pointing towards the sensor. n is the shininess coefficient (Phong, 1973).

$$\theta = COS^{-1}(\hat{r} \,.\, \hat{v}) \quad (3)$$

The specular radiance can then be calculated by substituting into the Phong model and integrating over the visible area and the solid angle concerned, considering that the sensor can only see the reflection if $\hat{r} \,.\, \hat{v} > 0$.

$$L = \int_{\hat{r} \,.\, \hat{v} > 0} I_i \cdot k_s \cdot (\hat{r} \,.\, \hat{v})^n d\Omega \quad (4)$$

1.4 Forward model

The simulation used a forward model which essentially maps the physical properties of a specular surface to the radiance field it produces when illuminated. This involves considering how the light interacts with the surface at various points and angles.

1.4.1 Key components of the forward model

The model takes into account the geometric shape of the surface and its material properties like reflectivity and roughness. For the light source, it considers the position, intensity, and distribution of the light source illuminating the surface. The model uses the law of reflection, which states that the angle at which light hits the surface is equal to the angle at which it is reflected. The angle measured normal to a surface.

1.4.2 Simulation of the Targets

The simulation utilizes a predetermined target surface described by the equation $P(x) = .2(X^4 - X^2)$. The mathematical model helps interpret the surface's geometric intricacies, which is crucial for analyzing specular reflection. The surface's detailed representation is built within the simulation framework, following closely to the prescribed forward model. The figures presented (Figure 2 and Figure 3) show the simulation output and the radiance response respectively.

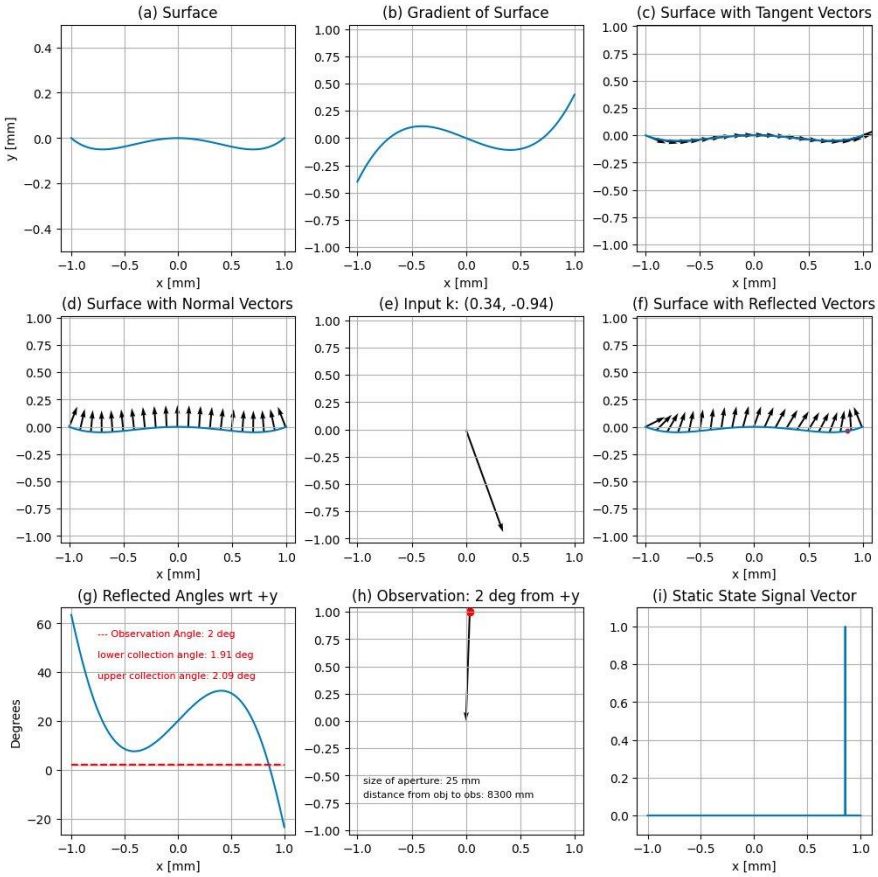

Figure 2: Target 1 Simulation

(Figure 2) illustrates the modeled surface derived from the equation $P(x) = .2(X^4 - X^2)$ in figure (a), and the path of incident light as per the forward model, providing a visual representation of the theoretical setup. The (Figure 2) represent each step taken in the model. (a) shows the predetermined surface. (b) shows the gradient or slope generated from each point on the surface. (c) represent the tangent vector at each point on the surface, calculated using the gradient. (d) illustrate the normal vector to each tangent vector. (e) detailed the incident angle. (f) represents the reflected vectors from the normal vectors as a dot product of the incident vectors. (g) shows the reflected angle with respect to the +y-axis. Figure (h) and (i) provide a further representation of this process. The model encompasses a total of 2048 sampling points on the surface and the number of observation angles is 1300. The cumulative results from this model is represented in the following (Figure 3).

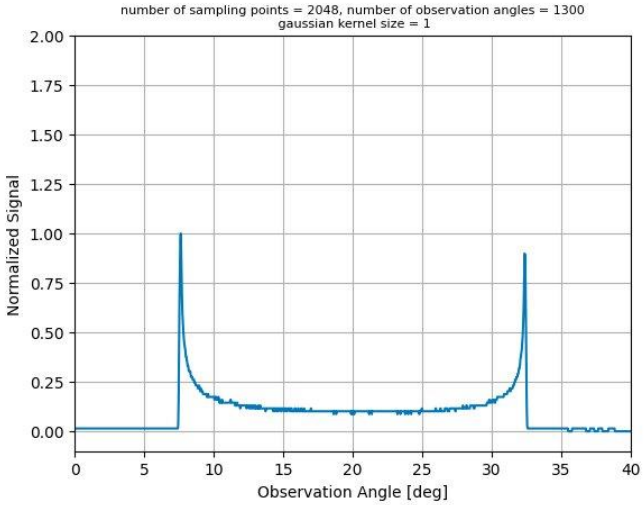

Figure 3: Target 1 Simulated Specular Reflection

(Figure 3) captures the resulting radiance patterns, providing empirical evidence of the simulation's effectiveness in replicating the expected specular reflection based on the redefining surface geometry. This only represents pure specular reflection without including any noise or diffuse reflection.

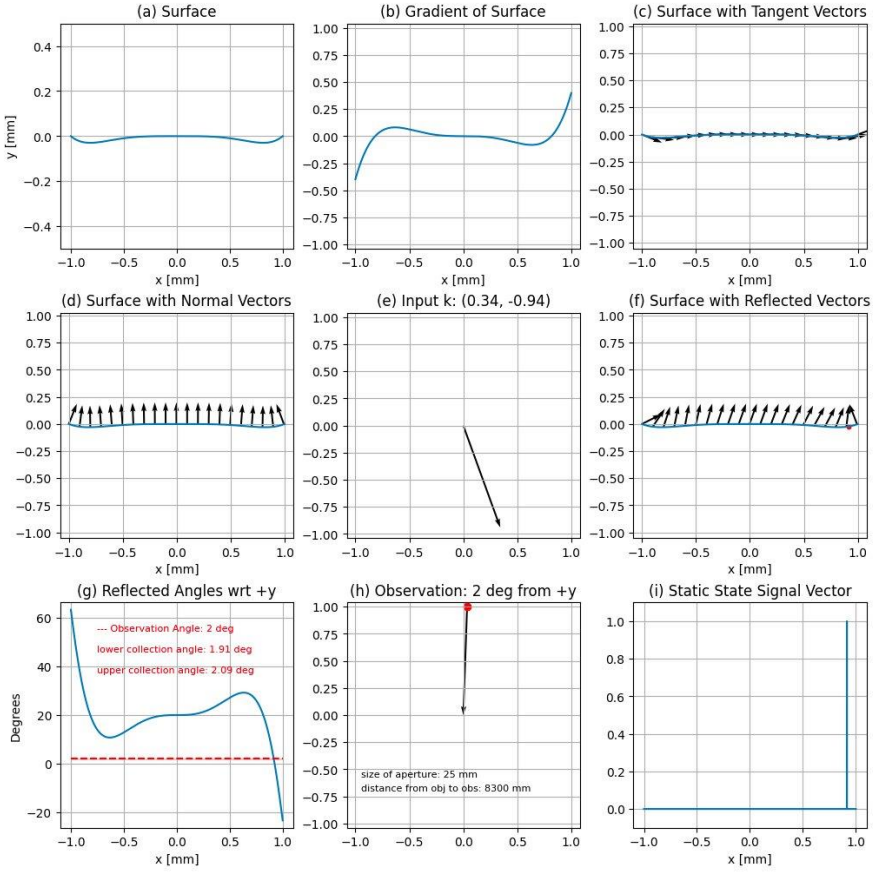

Figure 4: Target 2 Simulation

The surface in (Figure 4) is derived from the equation $P(x) = 0.2(X^6 - X^4)$.

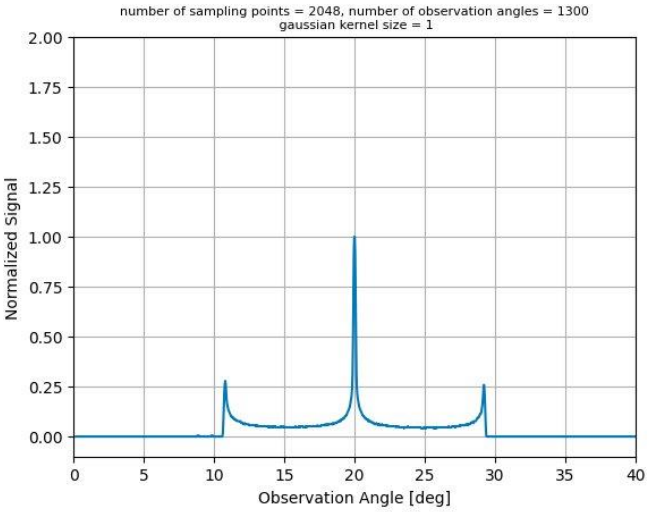

Figure 5: Target 2 Simulated Specular Reflection

Each target has its distinguished pattern, as represented in (Figure 3) and (Figure 5).

1.5 Experimentation

1.5.1 Lab experiment

In our laboratory experiment, a detailed investigation continued to validate the theoretical predictions related to specular reflections on predefined surface shapes. Utilizing a shaped sheet metal sheet, we simulated the specular reflection we expected to observe. This controlled setting allowed for an unambiguous examination of the specular reflection phenomena.

Figure 6: Lab Expermint Targets

When we transitioned from simulation to the actual experiment, the experimental data confirmed the simulated results. The experimental setup was carefully designed to replicate the simulated conditions with a light source that incident to the target and precise angular placement for the sensor (Figure 3). The sensor used in this experiment was the Basler 231 acA1440-220um, with a 4mm focal length at F/2.8. Upon illuminating the sheet metal surface, the target rotates 180^{o} by its vertical axis using a stage, and the sensor captures the reflected light.

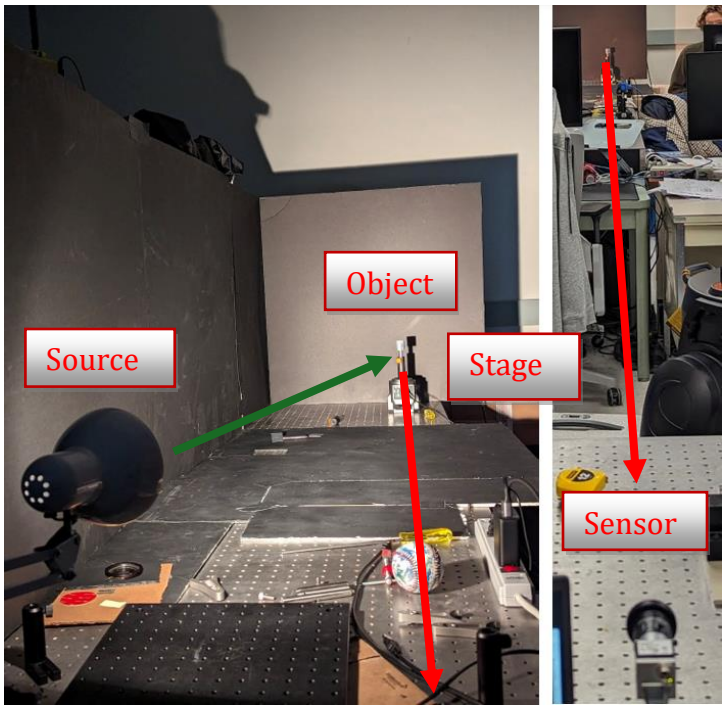

Figure 7: Lab test setup

Figure 8: The captured image from Target 1- one frame

The sensor was programmed to capture 148 frames throughout the experiment. Each frame was captured at 100 milliseconds, allowing it to obtain a detailed temporal resolution of the reflection patterns. This high-frequency capture rate is crucial because it enables the analysis of the transient behaviors of specular reflection as they vary while the target is rotating. The spatial resolution of the data captured was also a critical factor in the experiment. Each frame captured by the sensor spanned 7 pixels in width. This specific measurement of pixel width is significant as it relates to the sensor's ability to resolve the reflection pattern. As shown in (Figure 8), the yellow region is down-sampled (binned) to reach the unresolved region for this experiment.

The resulting data, as displayed in (Figure 9), exhibits the same two spikes that were apparent in the simulations shown in (Figure 3). The figure's horizontal axis (Slice) represents the captured frames, while the vertical axis denotes the signal intensity (Specular Reflections). The captured data includes noise and diffuse reflection, which are inherent in such measurements. This outcome aligns with the previously discussed simulated and experimental results, thereby validating our understanding of the interaction between light and the sheet metal surface used in the experiment. The team employed ImageJ software to conduct this analysis, enabling precise visualization and quantification of the specular reflections.

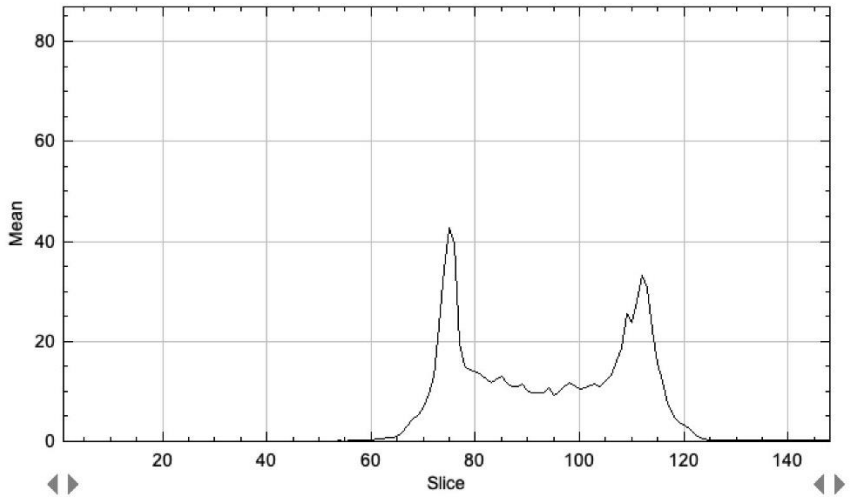

Figure 9: Target 1 - Specular reflection from the Lab experiment

The result from the second target is shown in (Figure 10), which match the results generated from the simulation (Figure 5). The three spikes are distinguishable with high peaks in the middle, confirming that each surface has a distinguished specular reflection.

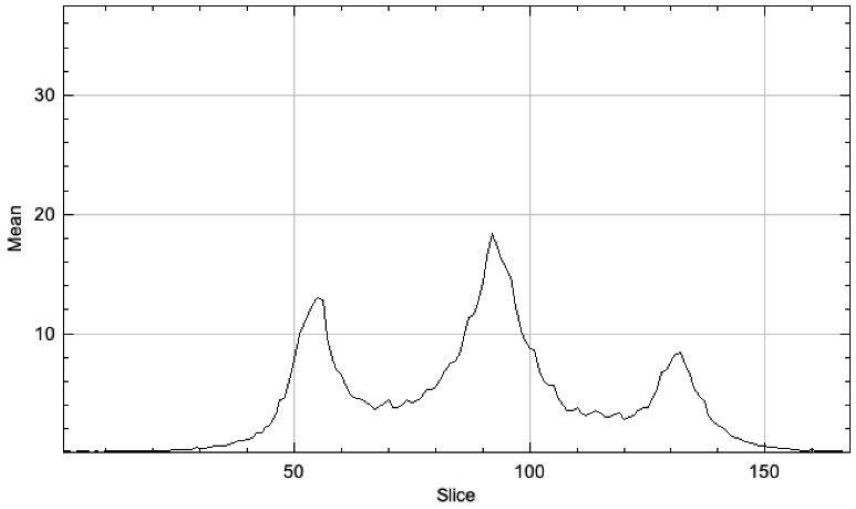

Figure 10: Target 2 - Specular reflection from the lab experiment

The experiment's findings reaffirm the prediction of our simulation's specular reflection. This finding paves the way for using such experimental approaches to characterize the reflective properties of various materials and surfaces with high fidelity.

Furthermore, the ability to predict and verify the specular reflection pattern for a known surface geometry holds significant implications for mapping targets of interest and implies that for remote sensing applications. It demonstrates that by carefully analyzing the reflection

patterns and accessing critical information about the object's surface characteristics—even when the object is unresolved at a distance.

1.5.2 Field experiment at 5 km

The second experiment expanded the scope of our investigation into specular reflection by conducting a long-range field test. The objective was to determine whether the distinct spike signature observed in laboratory conditions could be detected at a significant distance, thus simulating a realistic scenario to match remote sensing applications.

Experimental Setup

This experiment's range was 4.7 kilometers, with the setup positioned between a parking garage on E 6th St. & N. Warren Ave. in Tucson and Sentinel Peak, commonly known as A-Mountain. Figure 11. The experiment takes on the advantageous positioning provided by the urban topography, offering a clear line of sight between the two points, as shown in (Figure 12).

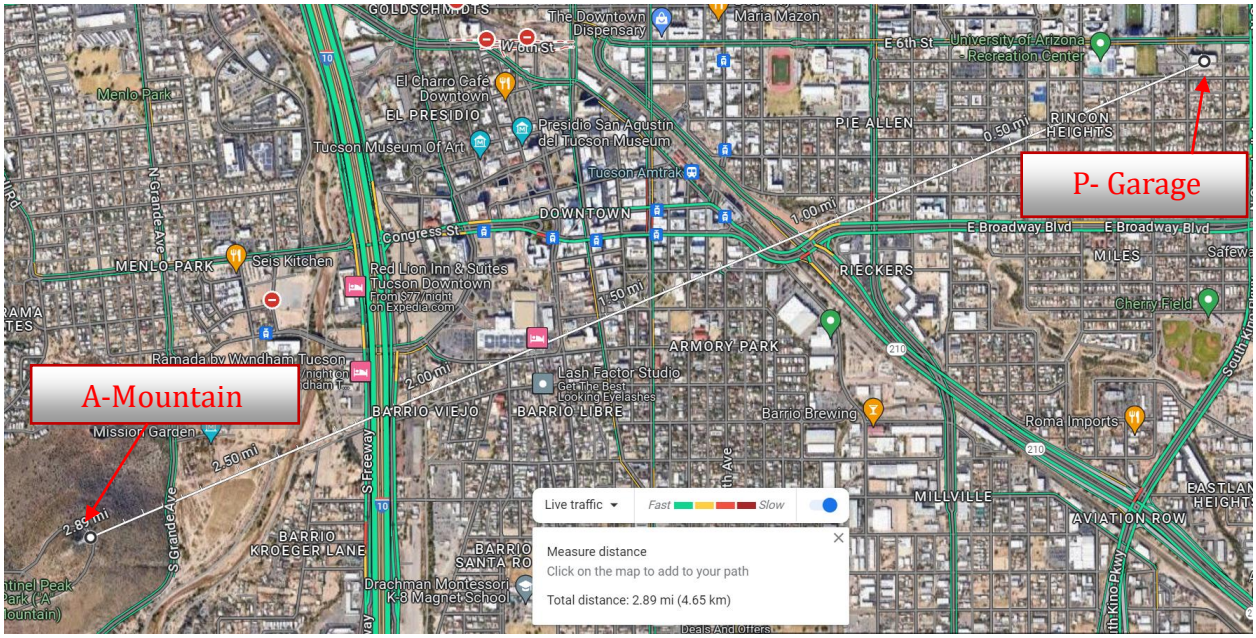

Figure 11: Filed experiment locations

Figure 12: Line of sight to A-mountain

For this experiment, we selected a SWIR (Short-Wave Infrared) camera, the Allied Vision VSWIR 1800 U-130, and a Basler ace UacA1440-220um (Visible Light) camera. Both were mounted on a CPC 1100 GPS (XLT) computerized telescope, chosen for its high sensitivity and precision, which are crucial for capturing detailed target reflections over long distances. Following the established laboratory procedure, the target was placed on a rotating stage capable of 180-degree rotation around its vertical axis. The primary light source for this experiment was the sun. The timing of the experiment was carefully planned to ensure that the target was positioned to receive sufficient sunlight for optimal reflection. The sensors were programmed to capture a high frame rate as the target rotated, ensuring continuous and detailed data collection throughout the experiment.

Table 1: Sensors Specification

Specification	SWIR	VIS
FOV (Degree)	0.13°	0.1°
F-num	10	10
IFOV (mRads)	0.00178	0.00121

Findings

In alignment with our lab results, we successfully detected the two spike shapes shown in (Figure 14) from Target 1 as in (Figure 6). Our instruments capture the reflected signal, matching the simulation and the lab experiment. This confirms that the distinctive specular reflection pattern can be observed and recognized even across the 4.7-kilometer distance, thus demonstrating the robustness of the reflection signature as a means of identification.

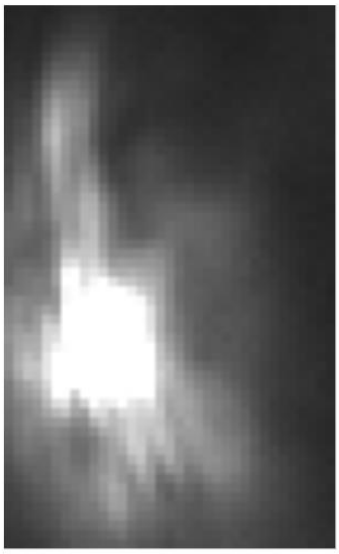

Figure 13: Target reflection from the sun at 4.7 km away in a single frame

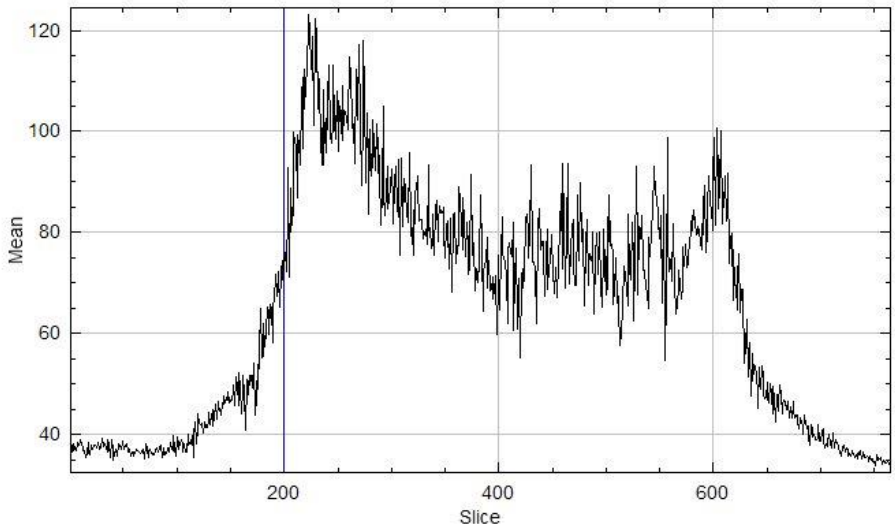

Figure 14: Specular reflection from the target

The SWIR camera demonstrated superior contrast performance compared to the VIS camera. The captured frames were analyzed similarly to the lab experiment, revealing the specular reflection pattern referred to in (Figure 15). The SWIR camera's heightened sensitivity

to infrared light allowed for a clearer detection of the spikes, which may have been obscured in the visible spectrum due to atmospheric conditions or sunlight scattering.

The experiment's success was further underscored by our ability to pinpoint the location of the target team. Their use of a mirror to reflect sunlight created a bright, detectable signal, which, when observed through the SWIR camera, was pronounced enough to locate them accurately. This finding has profound implications for search and rescue operations, where the ability to detect signals from great distances can be life-saving.

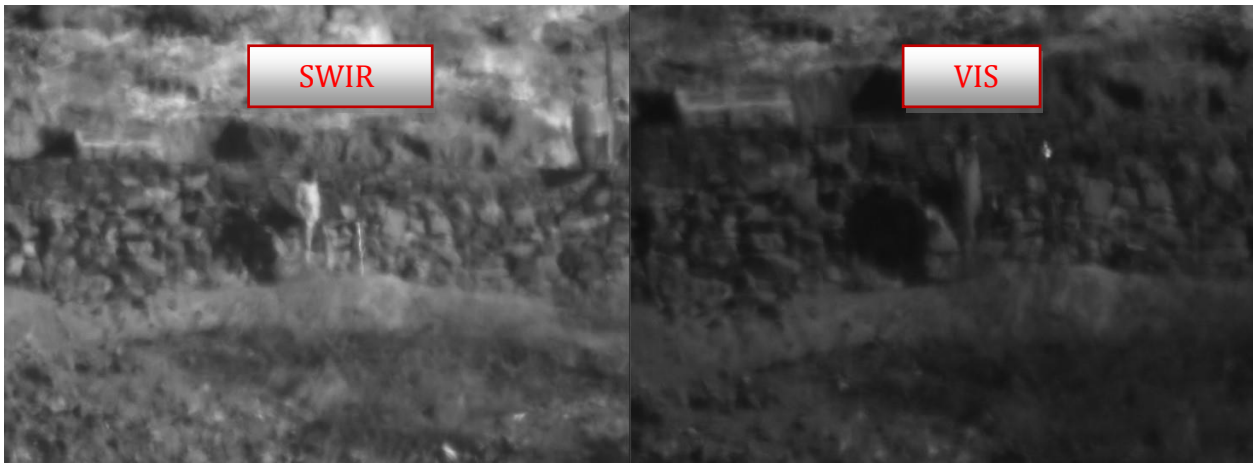

Figure 15: SWIR vs VIS

Expansion

The success of this field experiment signifies a leap forward in our ability to utilize specular reflections for remote sensing. By detecting the same spike signature that we observed in the laboratory from 4.7 kilometers away. This demonstrated the effectiveness of this method to be used in practical, real-world scenarios.

The implications of these findings are diverse. For instance, in a military context, this could translate to the ability to identify and track objects of interest based on their reflective signatures. It will enable the identification of vehicles or equipment from safe distances. In civil applications, this technology could be used to monitor wildlife or track environmental changes without the need for proximity that might disturb the natural setting or pose a risk to the monitoring team.

The superior performance of the SWIR camera highlights the importance of selecting the appropriate spectral band for observation, as different wavelengths can offer varying levels of detail and penetration through atmospheric interference, refer to (Figure 16) and (Figure 17). The following Modulation Transfer Function (MTF) is used to measure the performance of the SWIR and VIS against the turbulence effect. The following equation represents the atmospheric MTF (Driggers, 2022).

$$MTF_{se}(\xi) = exp\left[-57.53\left(\frac{\xi}{\lambda}\right)^{5/3} C_n^2 \lambda^2 R^{5/6}\left(1 - \left(\frac{\lambda\xi}{D}\right)^{1/3}\right)\right]$$

Where C_n^2 is the refractive index structure constant, which measures the strength of atmospheric turbulence. It directly influences the clarity that optical systems can image over distance. The variable ξ, representing the spatial frequency in cycles per radian, is critical in determining the resolution of the sensors. λ is the wavelength in meters, and R is the path length in meters. D is the aperture diameter of the system's sensor. This model allowed us to quantify the degradation of the image quality due to atmospheric turbulence. This insight directs future remote sensing endeavors to consider the spectral properties of their targets and the environment to optimize detection capabilities.

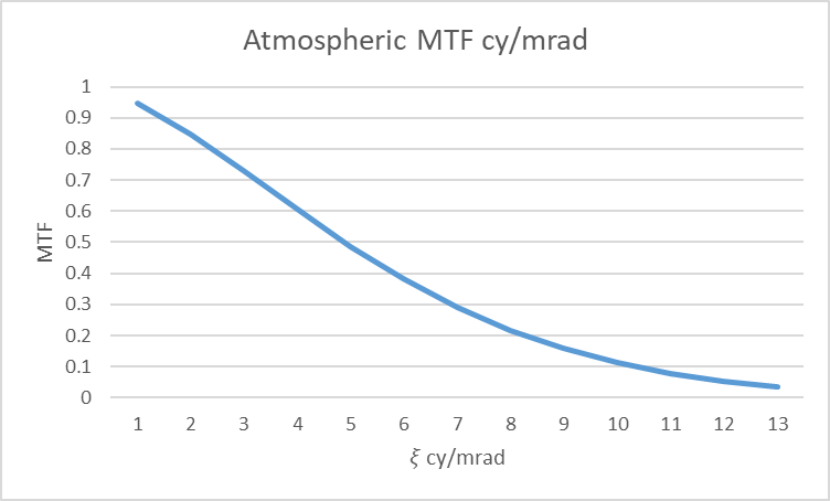

Figure 16: Turbulence MTF for SWIR Camera

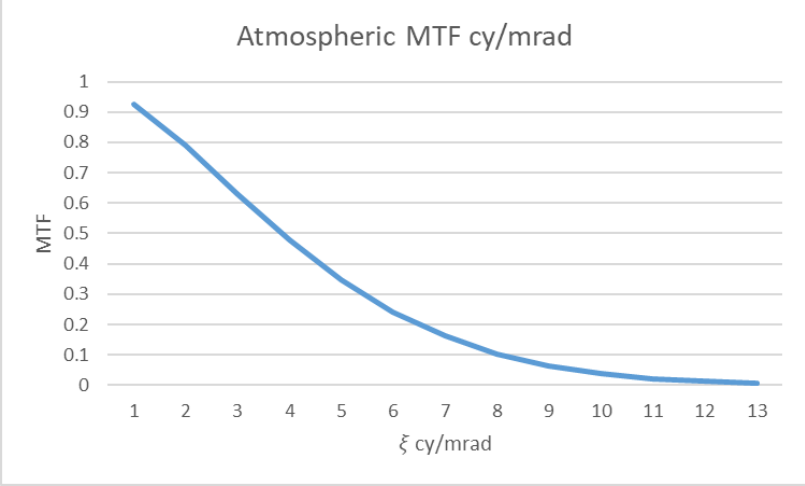

Figure 17: Turbulence MTF for Visible Camera

In summary, this field experiment validates theoretical and laboratory-based findings about specular reflections and opens up new avenues for the practical use of radiometry in remote identification and characterization. It enhances our observational capabilities beyond what conventional imaging methods can achieve.

1.5.3 Third Experiment

The third experimental attempt to push the boundaries of our research further into the region of long-range identification, targeting an expansive 27-kilometer distance from Sentinel Peak on A-Mountain to the Babad Do'ag Scenic Overlook in Tucson, as shown in (Figure 18) This trial was specifically designed to probe the limits of identification within the unresolved region, where the target objects are too small or too distant to be discerned as separate entities by the sensor.

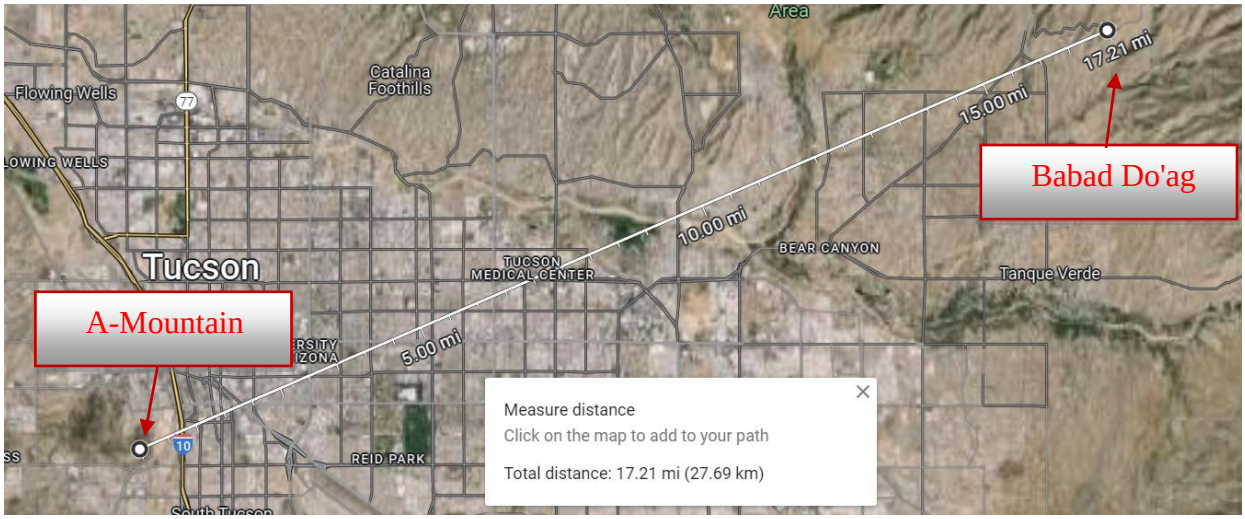

Figure 18: Long-range experiment locations

Performance Model

Using Night Vision Integrated Performance Model (NV-IPM), a performance model was created to evaluate the theoretical system's ability to detect the sun's reflection from the target. The NV-IPM is a versatile analytical tool used primarily for evaluating the performance of imaging systems. The system parameters and assumptions are provided in the following (Table 2) .

Table 2 : System Parameter

Target and Background	
Light Source	Direct Sunlight
Target Reflectivity	80%
Background Reflectivity	Light Rocks (400nm-2um)
Target Size	0.5 meter
Atmosphere	
C_n^2	1.0E-17
Modtran	1976 US Standard
Aerosol Model	Desert
Optical System	
Optical Transmission	89%
Effective Focal Length	2800 millimeter
Aperture Diameter	279 millimeter
Detector	
Pixel Size	5 micromerter

Horizontal Detector Count	1296
Vertical Detector Count	1032

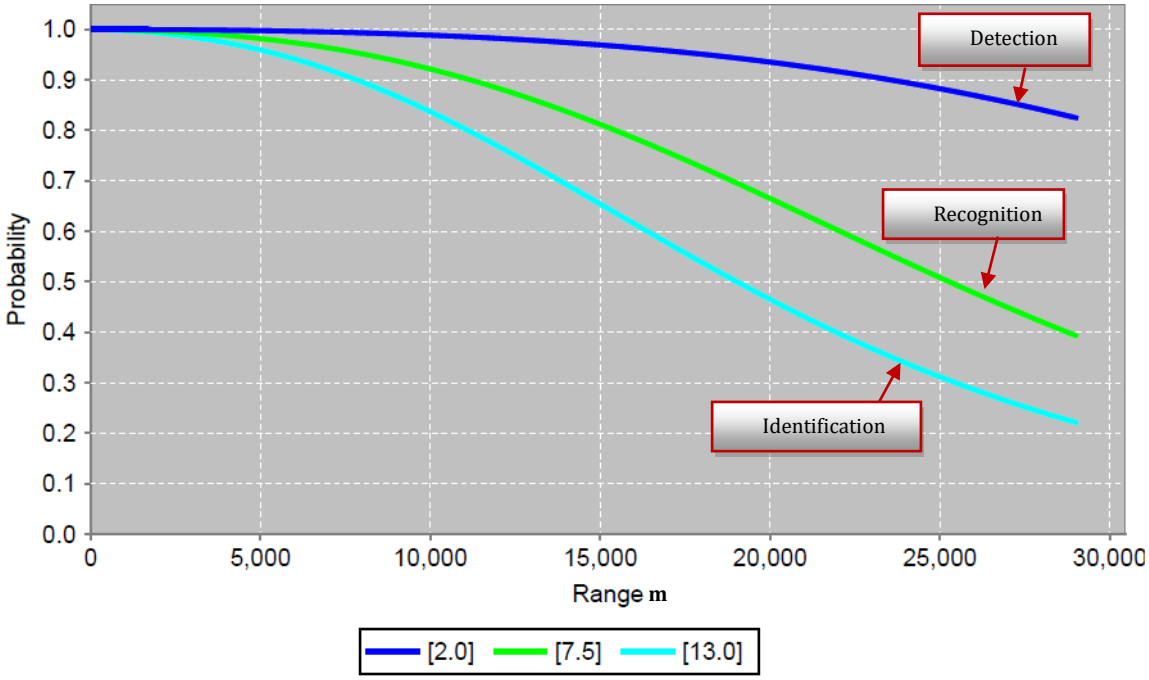

Figure 19: Probability of Task Performance - V50

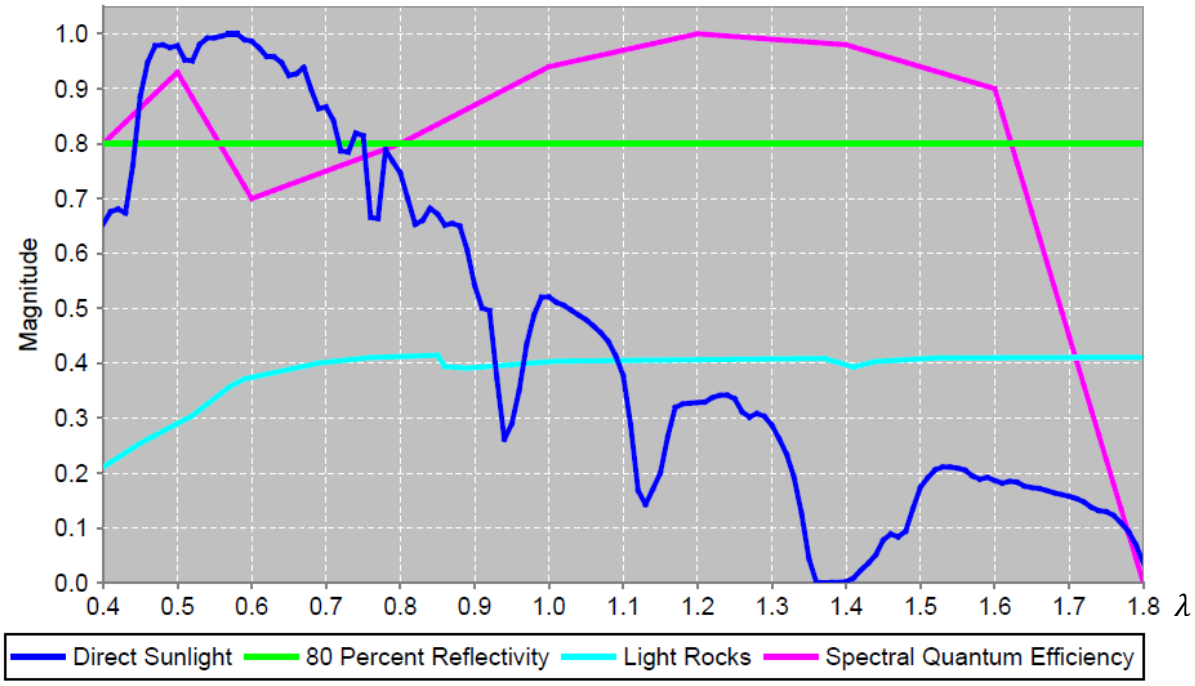

Figure 20 : Spectral Data

The performance metrics derived from the NV-IPM provided insightful data as shown in (Figure 19). The results indicated that the recognition accuracy measured to be 40 %, while identification accuracy was slightly lower at 25%. These statistics highlight a relativity-limited efficacy in identifying and recognizing distant targets, which poses challenges for operational decision-making based on this data alone.

Given these limitations, it becomes evident that relying solely on traditional imaging for distant object recognition and identification at such extended ranges may not be sufficient. In a scenario where precision and reliability in target identification are crucial, additional or alternative methods are necessary to enhance the overall efficacy of the sensing systems.

This is where the utility of specular reflection becomes particularly significant. (Figure 20) shows the spectral data for the experiment to give insight into the scene.

This model gives this experiment another goal where sufficient data from specular reflection is necessary.

Experimental Setup

The setup remained consistent with our previous long-range trial, employing the SWIR and VIS cameras in conjunction with the CPC 1100 GPS (XLT) computerized telescope. The capturing team was stationed on A-Mountain (Figure 21), while the target team positioned themselves at the Babad Do'ag Scenic Overlook, using sheet metal to produce a detectable specular reflection (Figure 22). This experiment had many trials to achieve the most accurate results. It used different target sizes to better represent the specular reflection. Among the trials, a crossed polarizer filter was used to evaluate the reduction of the noise from the scattered light.

Figure 21: Capturing team location

Figure 22: Target team location

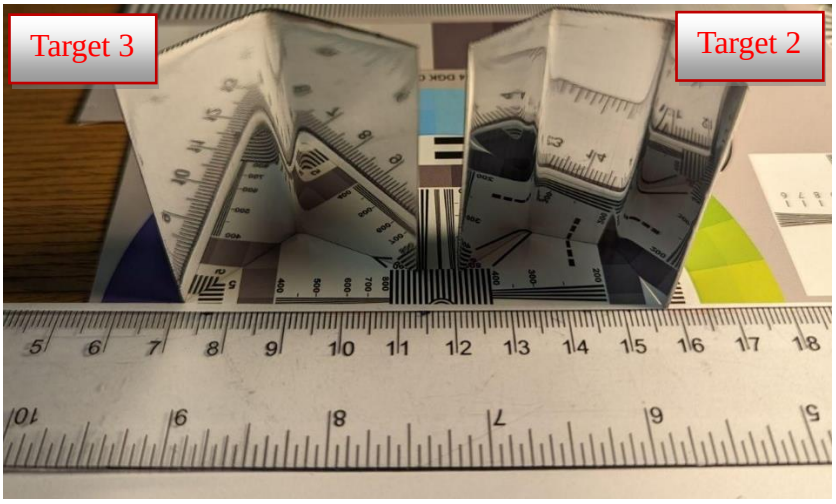

Figure 23: 50mm Targets

Findings

Despite the extended range and the target falling within the unresolved region for targets 2 and 3 (Figure 23), where the ground sampling distance is 5cm, our setup successfully captured a spike pattern in the reflected light from the target while rotating the target 180^{o} by a stage. This result is significant as it demonstrates our method's efficacy in detecting specular reflections over long distances, even when the target is not individually resolvable. For target 2, the result showed in (Figure 26) matches the simulation where the expected three spikes should be presented. The figure shows two rotations conforming to the repeatability.

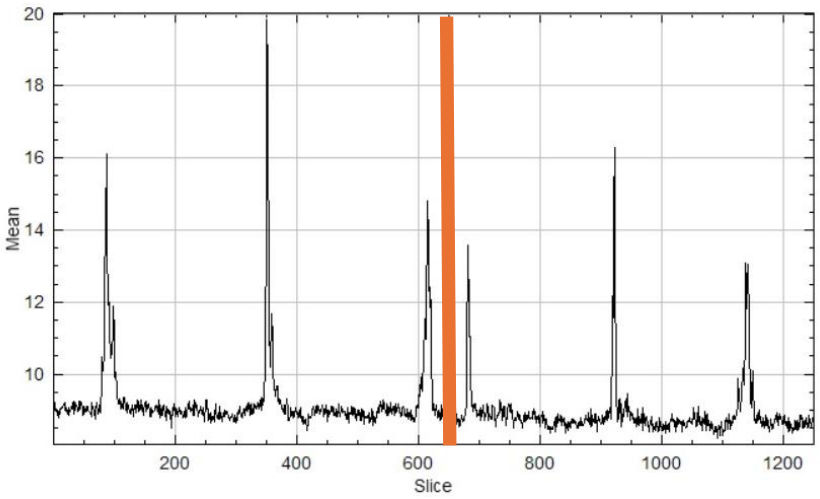

Figure 24: Specular reflection from Target 2

For target 1, the following (Figure 25) shows the sun's reflection. Even with a 0.5 m target, the classification is impassable by normal means. This confirms the NV-IPM model, where the property of identification falls below 25%.

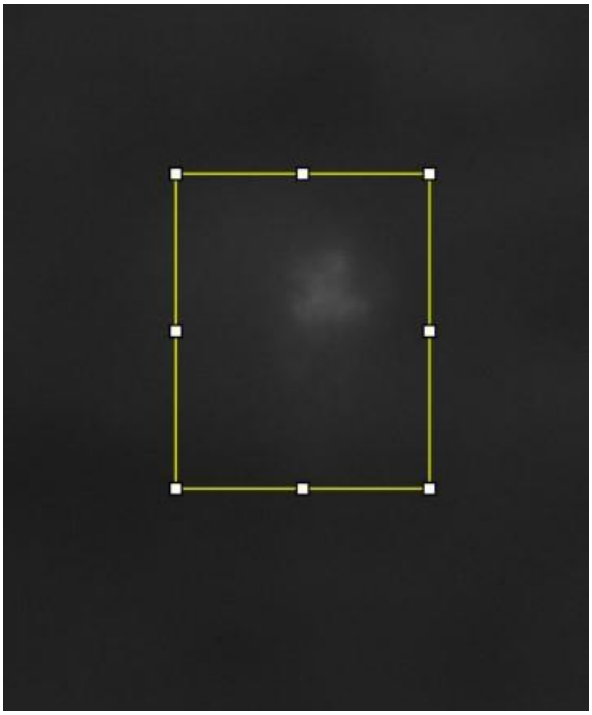

Figure 25: Target 1 reflection from the sun at 27 km

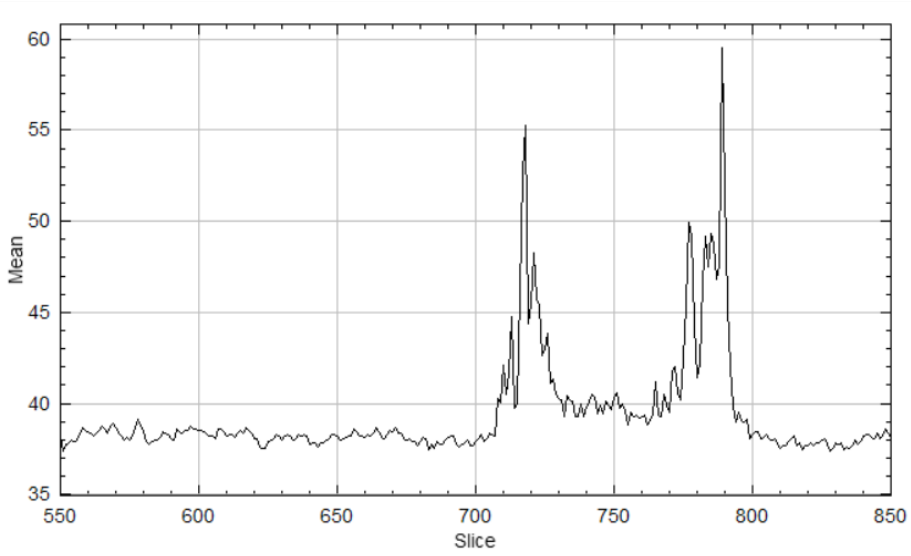

Figure 26: Specular reflection from Target 1

The result shown in (Figure 26) matches the simulation and other experiments where the expected two spikes should be presented.

The polarizer has effectively reduced the noise from the scattered light, making the specular reflection more distinguishable. Another benefit of the polarizer is reducing the blooming that is not reduced by lowering the exposure due to the limits of the camera dynamic range, refer to (Figure 27) .

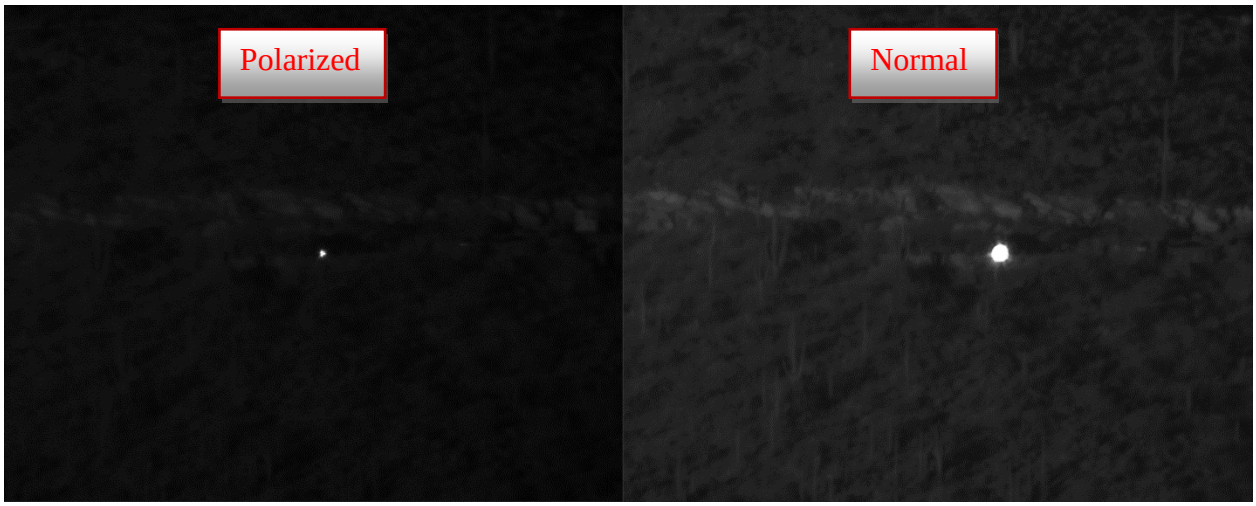

Figure 27: Polarizer effects at 27km

As this experiment extended to 27 km, the system became more sensitive to vibration. Vibration can significantly degrade the sharpness and clarity of an image by causing the optical elements or the entire system to move during exposure. This movement leads to a blurring effect, which is particularly pronounced at higher spatial frequencies. For low-frequency vibration, the effect on image quality depends on the point within the object motion cycle when exposure occurs. The wind and other mechanical movements blur the images and distort the data collected. A mitigation for future experiments is to use an active stabilizer.

1.6 Next Steps

The following steps of the research aim to design objects with defined specular reflections to act as calibration targets. These objects will enhance the precision of our classification algorithms by providing a controlled standard. This advancement could potentially used for the identification of friendly military assets such as troops, vehicles, and aircraft through unique optical signatures where a helmet or a vest to be designed in such a way to provide a unique signature.

Further development will involve the exploration of Extended SWIR (ESWIR), Mid-Wave Infrared (MWIR), and Long-Wave Infrared (LWIR) spectral bands. Each of these bands has its distinct propagation characteristics and interacts uniquely with the atmosphere, which could lead to improved identification capabilities under different environmental conditions. The most ambitious aspect of the research will be to integrate the refined classification algorithms into a staring array system for continuous observation to detect drones autonomously. The array camera will take images from different angles and generate a specular reflection signature of the target. This system will employ a database of analyzed specular reflections to accurately identify and track drones based on their unique specular signatures, using the Bidirectional Reflectance Distribution Function (BRDF) to model and predict the reflective properties of drones more accurately. This capability would mark a significant technological offering a passive, and non-intrusive method for airspace monitoring and security in both civilian and defense sectors.

The experiments confirm the practicality of utilizing specular reflections to identify distant, unresolved targets. Continuously improving the experimental design and analytical algorithms using methodological approaches will enhance the accuracy and practicality of remote sensing technologies. This progression will open new avenues in target identification, pushing the boundaries of what can be achieved through optical sensing.

References

1. Boreman, Glenn D. *Modulation Transfer Function in Optical and Electro-Optical Systems, Second Edition: Tt121*. 1st ed. Vol. v.TT121. Bellingham: SPIE, 2021. Print.
2. Driggers, Ronald G., Melvin H. Friedman, and John W. Devitt. *Introduction to Infrared and Electro-Optical Systems*. Third edition. N.p., 2022. Print.
3. Palmer, James M., Barbara G. Grant, and Society of Photo-optical Instrumentation Engineers. *The Art of Radiometry*. Bellingham, Wash. (1000 20th St. Bellingham WA 98225-6705 USA): SPIE, 2010. Print.
4. Lu, Shizhou et al. "A Novel Approach to Droplet's 3D Shape Recovery Based on Mask R-CNN and Improved Lambert–Phong Model." *Micromachines (Basel)* 9.9 (2018): 462. Web.
5. Tan, Kai, and Xiaojun Cheng. "Specular Reflection Effects Elimination in Terrestrial Laser Scanning Intensity Data Using Phong Model." *Remote sensing (Basel, Switzerland)* 9.8 (2017): 853. Web.
6. Seidaliyeva, Ulzhalgas et al. "Advances and Challenges in Drone Detection and Classification Techniques: A State-of-the-Art Review." *Sensors (Basel, Switzerland)* 24.1 (2023): 125. Web.
7. Guarnera, D. et al. "BRDF Representation and Acquisition." *Computer graphics forum* 35.2 (2016): 625–650. Web.
8. Yoo, Jung Hye et al. "A New Technique to Teach Basic Concepts of Refraction and Reflection of Light." Vol. 9666. SPIE, 2009. 96661O–96661O–6. Web.
9. Khorram, Siamak et al. "Future Trends in Remote Sensing." *Principles of Applied Remote Sensing*. Cham: Springer International Publishing, 2016. 277–285. Web
10. Phong, Bui Tuong. Illumination for Computer-Generated Images. N.p., 1973. Print.